Fast macroscopic thermal analysis for laser metal deposition. Application to multiphase steels

Daniel Weisz-Patrault

II International Conference on Simulation for Additive Manufacturing - Sim-AM 2019
F. Auricchio, E. Rank, P. Steinmann, S. Kollmannsberger and S. Morganti (Eds)

FAST MACROSCOPIC THERMAL ANALYSIS FOR LASER METAL DEPOSITION. APPLICATION TO MULTIPHASE STEELS.

Daniel WEISZ-PATRAULT*

*LMS, CNRS, École Polytechnique, Institut Polytechnique de Paris, F-91128 Palaiseau, France

Key words: Additive manufacturing, Phase transitions, Heat conduction, Semi-analytical solution

Abstract. Recently, a simplified macroscopic and semi-analytical thermal analysis of Laser Metal Deposition (LMD) has been submitted to publication. The model is fast enough to simulate the entire process. The proposed approach enables to compute: temperature, solidification and solid-state phase transitions kinetics. Process parameters, substrate characteristics and heat sources due to the enthalpy change during phase transitions are taken into account as well as convection due to the carrying and shielding gas. The present work exploits the proposed model to investigate the influence of some process parameters in order to determine whether complex multiphase steels (such as high strength steels) could be controllably obtained by LMD. Indeed, material properties of such steels are not only a matter of chemical composition but also and mostly a matter of phase proportions in a multiphase mixture (austenite, ferrite, pearlite, bainite and martensite). Within this framework, temperature control strategies during the process are numerically tested for a simple cylindrical geometry.

1 INTRODUCTION

Laser Metal Deposition (LMD) consists in injecting a stream of metallic powder that is molten by a laser beam in order to deposit material layer-by-layer on a substrate [1, 2]. The LMD process induces very specific temperature history including very high temperature gradients (near the molten pool) and thermal cycling. Both the microstructure formation/evolution (solidification, solid state phase transitions, grain mobility etc.) and the formation of residual stresses are driven by thermal conditions during the process. Therefore, significant efforts have been made to simulate accurately, at the macroscopic scale, both temperature evolutions and solidification kinetics. However, macroscopic modeling of such processes is computationally costly [3–12]. The order of magnitude of computation cost for relatively small parts is several tens of hours. This hinders the development of efficient numerical optimization of process parameters in order to reach microstructure and material properties requirements.

Recently, a simplified macroscopic and semi-analytical thermal analysis of LMD has been submitted to publication [13]. The approach relies on a semi-analytical solution of the transient heat conduction problem in a two-dimensional multilayer composite (r, z radial and vertical coordinates). The solution derivation extends previous analytical thermal analysis on composites (e.g.,[14, 15]). The model enables us to efficiently compute temperature, solidification and

solid-state phase transitions kinetics in the whole part. Powder melting is not simulated, as molten metal is directly deposited on top of the already existing layers. However, several other aspects have been taken into account such as some process parameters (e.g., laser speed and power etc.), substrate characteristics (e.g., thickness and material properties), heat sources due to the enthalpy changes during phase transitions and forced convection due to the gas flow (used for carrying the powder and for shielding). In addition, the laser power is partly transmitted to the top layer of the already existing part.

In this contribution, the recently proposed model [13] is exploited to investigate the influence of some process parameters in order to determine whether complex multiphase steels (such as high strength steels) could be controllably obtained by LMD. Indeed, material properties of such steels are not only a matter of chemical composition but also and mostly a matter of phase proportions in a multiphase mixture (austenite, ferrite, pearlite, bainite and martensite). Within this framework, temperature control strategies during the process are numerically tested for a simple cylindrical geometry (even though the simulation strategy applies to arbitrary shapes in the horizontal plane and to arbitrary laser paths: continuous, back and forth etc.).

2 MODEL STRATEGY AND ASSUMPTIONS

The model developed in [13] relies on a semi-analytic solution of the unsteady and nonlinear heat equation. The general strategy is summarized in this section. In addition, the proposed solution is obtained by introducing some assumptions that are also recalled for sake of clarity. Further details and all mathematical developments are given in [13].

Volumetric heat sources due to the enthalpy changes during phase transitions arise as a right side term in the unsteady heat equation. As these heat sources strongly depends on the temperature field, the heat equation is non linear. This issue is overcome by an alternating scheme. Indeed, the heat equation becomes linear and easier to solve if the right side term is imposed (fixed to a known evolution). Thus, a first estimation of the temperature field is performed with a right side term arbitrarily set to zero. Then, the obtained estimated temperature field is used as inputs of a simple phase transition model detailed in section 3 and based on Johnson-Mehl-Avrami-Kolmogorov (JMAK) equation. Phase proportion rates are then used to compute the right side term of the heat equation and a new estimation of the temperature field is computed on this basis. This procedure is repeated until convergence.

Despite the fact that a nonlinear problem is solved as a succession of linear problems, the unsteady linear heat equation remains difficult to solve analytically mostly because of geometrical complexity and time dependency of the domain. Indeed, as new mass is regularly added to the part during the process, the support domain of the heat equation is strongly time dependent. To overcome these geometrical difficulties, the main assumption is to neglect heat fluxes along the tangent direction of the laser path (denoted by χ). That is to say that successive points on χ can be considered as independent. The validity of this assumption is questionable in the vicinity of the molten pool where temperature gradients are very significant in all directions. However, at the scale of the part, as molten metal is deposited at very high temperature on top of a relatively cold multilayer structure, heat fluxes along the vertical direction prevail.

This assumption leads to consider several independent computations at different positions

on the path χ. Each of these computation points consists in multilayer 2D structure in the (r,z) plane, where r is the radial coordinate (thickness direction) and z the vertical coordinate. The number of layers gradually increases as metal deposition goes on. Each computation point is characterized by (i) the radius of curvature of the path χ at the corresponding position and (ii) the different times of metal deposition on top of the multilayer structure denoted by $(t_1,\cdots,t_{N+1})$ (where N is the final number of layers). The simulation strategy consists in solving analytically the heat equation for each computation point on each time interval $[t_n,t_{n+1}]$ $(1\leq n\leq N)$. Thus, each computation point requires N sub-computations that are simply connected to each other by setting the initial condition on the time interval $[t_n,t_{n+1}]$ as the final condition on the previous time interval $[t_{n-1},t_n]$. It should be noted that for the same geometry different laser paths and dwell times can be simulated through different $(t_1,\cdots,t_{N+1})$. The layer thickness $h_r=0.75$ mm and height $h_z=0.2$ mm are fixed parameters that can be measured.

For sake of simplicity, the power per unit area brought to the system by the radiative term and by the laser is modeled as a power per unit volume. In addition, the gas flow increases significantly the heat transfer coefficient for all layers under the flow. However, the mathematical solution is based on constant heat transfer coefficient (denoted by H). Thus, temperature losses due to the gas flow are also modeled through the introduction of an additional negative volumetric heat source. On this basis, the unsteady heat conduction equation reads:

$$\frac{\partial^2 T^{(i)}}{\partial r^2}+\frac{1}{r}\frac{\partial T^{(i)}}{\partial r}+\frac{\partial^2 T^{(i)}}{\partial z^2}-\frac{1}{D}\frac{\partial T^{(i)}}{\partial t}=\frac{Q^{(i)}(t)}{\lambda} \tag{1}$$

where $T^{(i)}$ is the temperature in the layer (i), D ($\mathrm{m}^2.\mathrm{s}^{-1}$) is the thermal diffusivity. In this contribution, material parameters (D diffusivity and λ thermal conductivity) are assumed to be temperature independent for sake of simplicity. However, temperature dependent properties are considered in [13]. The volumetric heat source $Q^{(i)}$ contains four contributions: the radiative term, the heat source due to the enthalpy change during phase transition, the volumetric heat source Q_{beam} in the top layer of the already existing part due to the laser and the volumetric negative heat source $Q^{(i)}_{\text{gas}}$ associated to the local increase of the heat transfer coefficient due to the gas flow. A Gaussian model adapted from [7] is used for the layer $i=n-1$:

$$Q_{\text{beam}}(t)=-\frac{2\eta_{\text{beam}}P_{\text{beam}}}{\pi h_z R^2_{\text{beam}}}\exp\left(-2V^2_{\text{beam}}\frac{(t-t_n)^2}{R^2_{\text{beam}}}\right) \tag{2}$$

where η_{beam} is the absorption coefficient, P_{beam} is the laser power, R_{beam} is the laser radius and V_{beam} is the laser speed. A Gaussian approximation similar to (2) is introduced for $Q^{(i)}_{\text{gas}}$:

$$Q^{(i)}_{\text{gas}}(t)=\widetilde{Q}_{\text{gas}}\exp\left(-2V^2_{\text{beam}}\frac{(t-t_n)^2}{R^2_{\text{gas}}}\right) \tag{3}$$

where $\widetilde{Q}_{\text{gas}}$ is a power per unit volume and R_{beam} is a characteristic length controlling the affected area by the gas flow.

The substrate is modeled in a simplified way. It is assumed that the substrate temperature T_{sub} is constant on each time interval $[t_n, t_{n+1}]$. The substrate temperature T_{sub} is updated at the end of the n-th sub-computation according to the total energy received during the time interval $[t_n, t_{n+1}]$. Thus, boundary conditions read:

$$\begin{aligned}
(a): &\begin{cases} \lambda \dfrac{\partial T^{(i)}}{\partial r} = H\left(T^{(i)} - T_{\text{ext}}\right) & r = R_{\text{inf}} \quad (1 \leq i \leq n) \\ \lambda \dfrac{\partial T^{(i)}}{\partial r} = -H\left(T^{(i)} - T_{\text{ext}}\right) & r = R_{\text{sup}} \quad (1 \leq i \leq n) \end{cases} \\
(b): &\begin{cases} \lambda \dfrac{\partial T^{(1)}}{\partial z} = H_{\text{sub}}\left(T^{(1)} - T_{\text{sub}}\right) & z = Z^{(0)} \\ \lambda \dfrac{\partial T^{(n)}}{\partial z} = -H\left(T^{(n)} - T_{\text{ext}}\right) & z = Z^{(n)} \end{cases} \\
(c): &\begin{cases} T^{(i)} = T^{(i+1)} & z = Z^{(i)} \quad (1 \leq i \leq n-1) \\ \dfrac{\partial T^{(i)}}{\partial z} = \dfrac{\partial T^{(i+1)}}{\partial z} & z = Z^{(i)} \quad (1 \leq i \leq n-1) \end{cases}
\end{aligned} \tag{4}$$

where $Z^{(i)}$ denotes the interfaces in the multilayer structure, R_{inf} and R_{sup} denote the inner and outer radius respectively. In addition, H_{sub} denotes the heat transfer coefficient between the part and the substrate.

Mathematical developments to solve analytically the heat equation (1) with boundary conditions (4) are not detailed in this paper. Interested readers are therefore referred to [13].

3 PHASE TRANSITIONS

The phase transition model simply consists in JMAK equation or Koistinen-Marburger equation. Multiphase steel is considered. Each phase transition is characterized by a temperature range. Phase proportions are denoted by X_{liq}, X_{aus}, X_{fer}, X_{per}, X_{bai} and X_{mar} (liquid, austenite, ferrite, pearlite, bainite and martensite respectively). Solidification and fusion are approximated by a temperature dependent exponential model, for $T \in \left[T_{\text{sol}}, T_{\text{liq}}\right]$:

$$X_{\text{aus}} = 1 - \exp\left(-k_{\text{liq}}\left(T_{\text{sol}} - T\right)^{n_{\text{liq}}}\right) \tag{5}$$

where T_{sol} is the solidus temperature and T_{liq} the liquidus temperature. The identification based on the data given in [7] leads to $k_{\text{liq}} = 0.02$ and $n_{\text{liq}} = 1.22$. For austenite to ferrite, pearlite and bainite phase transitions, the classic JMAK equation is used. Phase proportions X_{fer}, X_{per} and X_{bai} are initially set to zero and are updated by computing the increase of phase proportion denoted by ΔX_ϕ:

$$\Delta X_\phi = X_{\text{aus}}\left[1 - \exp\left(-k_\phi\left(t - t_\phi\right)^{n_\phi}\right)\right] \tag{6}$$

where ϕ stands for ferrite, pearlite or bainite and k_ϕ and n_ϕ are the Avrami coefficients assumed to be independent on temperature and t_ϕ is the time when the phase transition starts. Furthermore, for the martensitic phase transition the classic Koistinen-Marburger equation is used. Consider ΔX_{mar} the phase proportion increase of martensite during cooling, for $T \leq \text{MS}$:

$$\Delta X_{\text{mar}} = X_{\text{aus}}\left[1 - \exp\left(\alpha_{\text{MS}}\left(T - \text{MS}\right)\right)\right] \tag{7}$$

where MS is the temperature start of martensite phase transition and α_{MS} a coefficient. With intense thermal cycling, the material is significantly reheated after cooling and may reach the temperature of austenitization. As heating rates are very high during the LMD process it seems sufficient to use an exponential interpolation similar to (5). Consider ΔX_{aus} the phase proportion increase of austenite during reheating, for $T \in [\mathrm{AE}_3, T_{\mathrm{aus}}]$:

$$\begin{cases} \Delta X_{\mathrm{aus}} = X\left[1-\exp\left(-k_{\mathrm{aus}}\left(T_{\mathrm{aus}}^{\mathrm{start}}-T\right)^{n_{\mathrm{aus}}}\right)\right] \\ X = X_{\mathrm{fer}}+X_{\mathrm{per}}+X_{\mathrm{bai}}+X_{\mathrm{mar}} \end{cases} \tag{8}$$

where T_{aus} is the temperature end of austenitization and AE_3 is the temperature start of austenite to ferrite phase transition (we consider in this paper that it is also the temperature start of austenitization).

4 RESULTS

In this section the model developed in [13] is used to analyze different fabrication strategies with respect to the formation of multiphase microstructures. Would it be possible to control the formation of predefined multiphase arrangements during the LMD process ? Material parameters and process parameters (excepted those tested in this paper) are extracted from [13]. Phase transition parameters are also extracted from [13] and do not correspond to a specific steel, but are coherent with multiphase steels. Following computations explore the idea of tailoring phase proportions by controlling substrate temperature and other process parameters. Thus, the substrate temperature is assumed to be controllable. The development of a real physical system enabling to adjust in real time the substrate temperature is not broached in this contribution. The main difficulty to favor austenite to ferrite, pearlite or bainite phase transformations is that those transitions are driven by carbon diffusion, hence slow evolutions of the corresponding phase proportions. Thus, the challenge is to maintain the part in the temperature range corresponding to these diffusive phase transitions during a sufficient amount of time. Three parameters are tested to achieve this objective: substrate temperature, laser speed and dwell time. All simulations consist in a 100 layers cylinder with 20 mm inner radius. Computations parameters are listed in table 1. The first computation is used as a reference to compare to other strategies. For each computation listed in table 1, the temperature at different fixed locations

Table 1: Computations

Computation	Substrate temperature (K)	Laser speed ($\mathrm{mm.s^{-1}}$)	Dwell time (s)
1	700	30	0
2	700	30	40
3	700	3	0

is given in figures 1, 4 and 7. The whole temperature field is also given at different times in figures 2, 5 and 8. Finally, the most significant phase proportion fields are given at different times in figures 3, 6 and 9. The last phase proportion field is the final phase mixture of the part. Further evolutions may be obtained with heat treatments.

The reference computation presented in [13] shows that without substrate temperature control, cooling rates are very fast and mostly martensite can be formed. (Of course for austenitic steels such as the widely used stainless steel 316L, mostly austenite is formed). The first computation listed in table 1 only consists in controlling the substrate temperature fixed at 700 K (with the same process parameters). Cooling rates are very similar as the those obtained for the reference computation. The part is globally in the austenite temperature range during the fabrication. Then, pearlite slowly starts to form during cooling to 700 K (around 1 min), then bainite is produced as the temperature is maintained at 700 K. The part is finally mostly composed of bainite.

More complex multiphase mixtures are obtained for the second computation, by introducing a dwell time. The main effect of combining the substrate temperature control and a long dwell time is that the part is in the pearlite or bainite temperature range for a sufficient amount of time during the fabrication. Similar phase proportions of pearlite and bainite are obtained. However, it is clear from figure 6 that the phase proportion field is not homogenous in the part. The third computation strategy consists in maintaining the substrate temperature at 700 K and decreasing the laser speed by a factor 10. This idea is similar as the second computation: lengthen the duration of the build so that slow diffusive phase transitions have time to occur. The difference is that the gas flow has been assumed to stop during dwell time although it is continuous with a low speed build. Thus, the cooling effect of the gas flow is very significant as shown in figures 7 and 8. This leads to a different multiphase mixture mostly composed of bainite and martensite as shown in figure 9. However, as for the second computation, the phase proportion fields are not homogenous in the part.

5 CONCLUSION

In this paper, a fast macroscopic model analyzing thermal evolution coupled with phase transitions during laser metal deposition process has been used to determine whether multiphase steel could be processed without further thermal treatment. Indeed, overall material properties do not only depend on the chemical composition but also on the multiphase mixture that is obtained during the process. Three sets of process parameters have been tested, assuming a hypothetical control of the substrate temperature. Very distinct multiphase mixtures have been obtained, which indicates that the proposed fast numerical strategy could be used to optimize process parameters in order to reach the targeted microstructure. However, a difficulty remains as the phase proportion fields are inhomogeneous in the part.

References

[1] William E Frazier. Metal additive manufacturing: a review. *Journal of Materials Engineering and Performance*, 23(6):1917–1928, 2014.

[2] Tarasankar DebRoy, HL Wei, JS Zuback, T Mukherjee, JW Elmer, JO Milewski, Allison Michelle Beese, A Wilson-Heid, A De, and W Zhang. Additive manufacturing of metallic components–process, structure and properties. *Progress in Materials Science*, 92:112–224, 2018.

[3] Liang Wang, Sergio D Felicelli, and James E Craig. Thermal modeling and experimental validation in the lens tm process. In *18th Solid Freeform Fabrication Symposium. Austin, TX*, pages 100–111, 2007.

[4] Heng Liu. *Numerical analysis of thermal stress and deformation in multi-layer laser metal deposition process*. PhD thesis, Missouri University of Science and Technology, 2014.

[5] Guillaume Marion, Georges Cailletaud, Christophe Colin, and Matthieu Mazière. A finite element model for the simulation of direct metal deposition. In *International Congress on Applications of Lasers & Electro-Optics*, volume 1, pages 834–841. LIA, 2014.

[6] Erik R Denlinger and Pan Michaleris. Effect of stress relaxation on distortion in additive manufacturing process modeling. *Additive Manufacturing*, 12:51–59, 2016.

[7] Jacob Smith, Wei Xiong, Jian Cao, and Wing Kam Liu. Thermodynamically consistent microstructure prediction of additively manufactured materials. *Computational mechanics*, 57(3):359–370, 2016.

[8] Trevor Keller, Greta Lindwall, Supriyo Ghosh, Li Ma, Brandon M Lane, Fan Zhang, Ursula R Kattner, Eric A Lass, Jarred C Heigel, Yaakov Idell, et al. Application of finite element, phase-field, and calphad-based methods to additive manufacturing of ni-based superalloys. *Acta materialia*, 139:244–253, 2017.

[9] Qiang Chen, Gildas Guillemot, Charles-André Gandin, and Michel Bellet. Three-dimensional finite element thermomechanical modeling of additive manufacturing by selective laser melting for ceramic materials. *Additive Manufacturing*, 16:124–137, 2017.

[10] DongYun Zhang, Zhe Feng, ChengJie Wang, Zhen Liu, DongDong Dong, Yan Zhou, and Rui Wu. Modeling of temperature field evolution during multilayered direct laser metal deposition. *Journal of Thermal Spray Technology*, 26(5):831–845, 2017.

[11] Cengiz Baykasoglu, Oncu Akyildiz, Duygu Candemir, Qingcheng Yang, and Albert C To. Predicting microstructure evolution during directed energy deposition additive manufacturing of ti-6al-4v. *Journal of Manufacturing Science and Engineering*, 140(5):051003, 2018.

[12] M Biegler, B Graf, and Michael Rethmeier. In-situ distortions in lmd additive manufacturing walls can be measured with digital image correlation and predicted using numerical simulations. *Additive Manufacturing*, 20:101–110, 2018.

[13] Daniel Weisz-Patrault. Fast macroscopic simulation of laser metal deposition process. thermal analysis coupled with phase transitions. *Submission*, 2019.

[14] F De Monte. Unsteady heat conduction in two-dimensional two slab-shaped regions. exact closed-form solution and results. *International Journal of Heat and Mass Transfer*, 46(8):1455–1469, 2003.

[15] Daniel Weisz-Patrault. Coupled heat conduction and multiphase change problem accounting for thermal contact resistance. *International Journal of Heat and Mass Transfer*, 104:595–606, 2017.

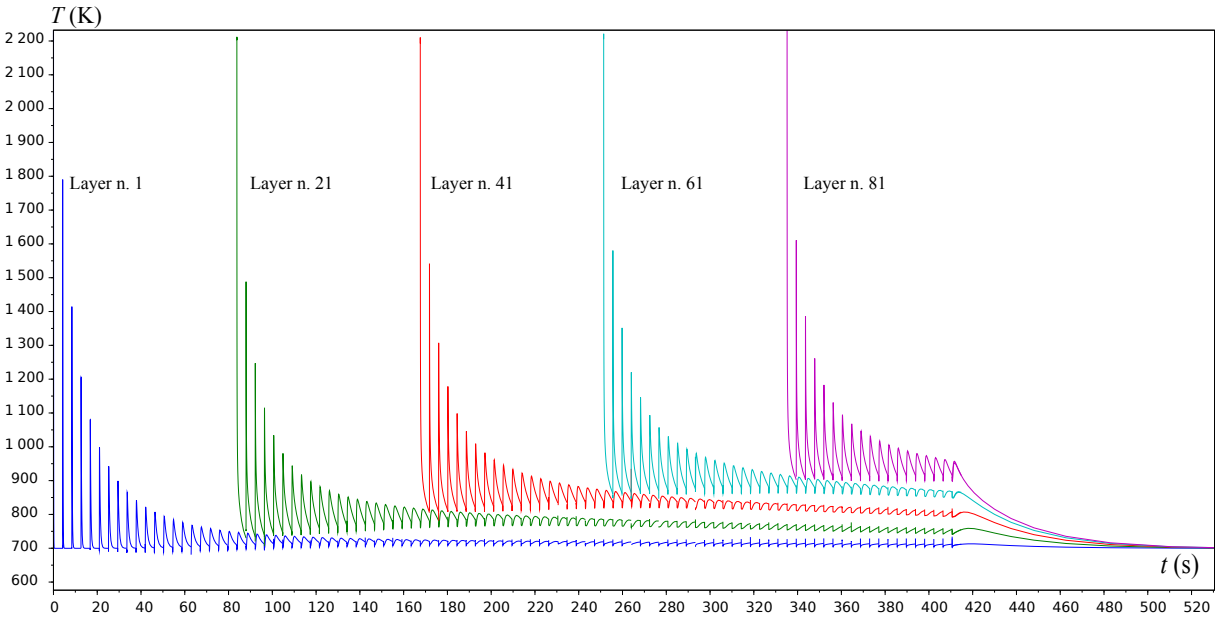

Figure 1: Temperature evolution of some layers, computation 1

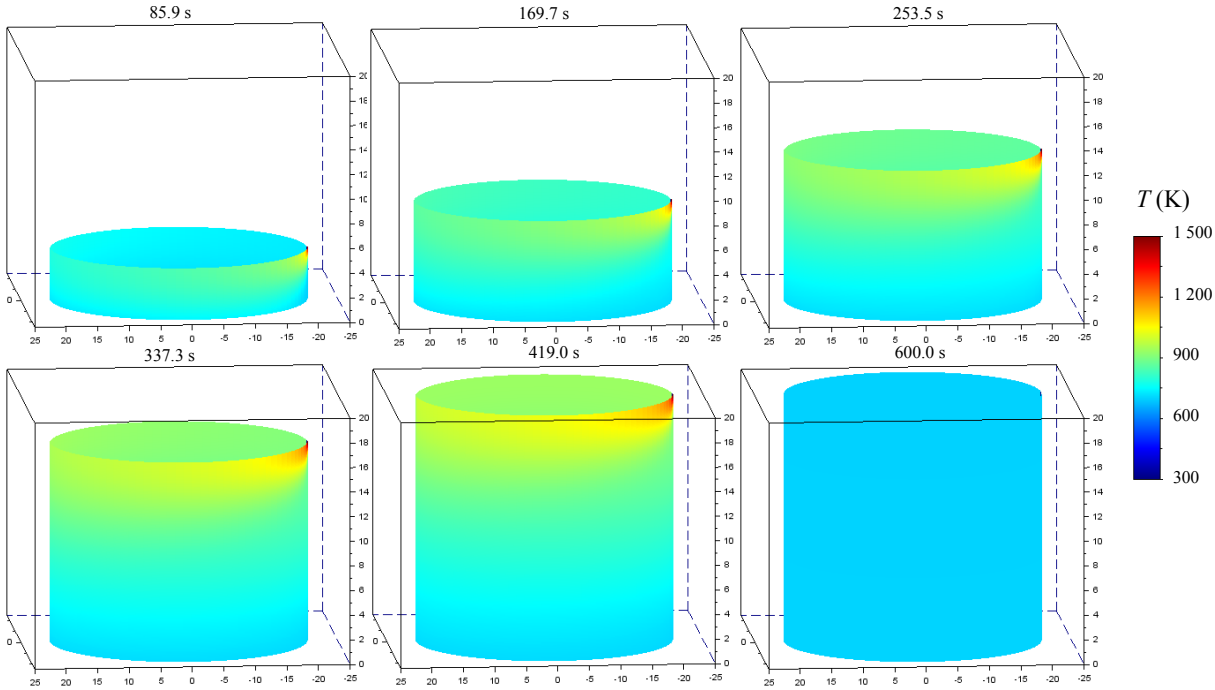

Figure 2: Temperature field, computation 1

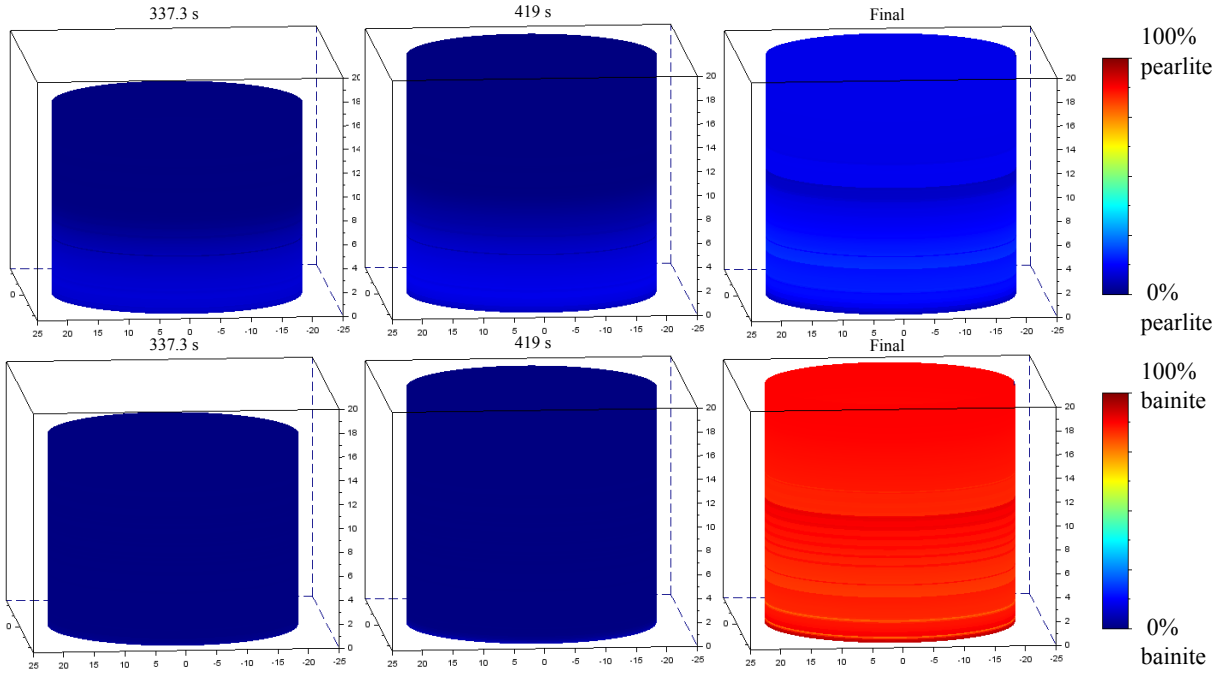

Figure 3: Phase proportion field, computation 1

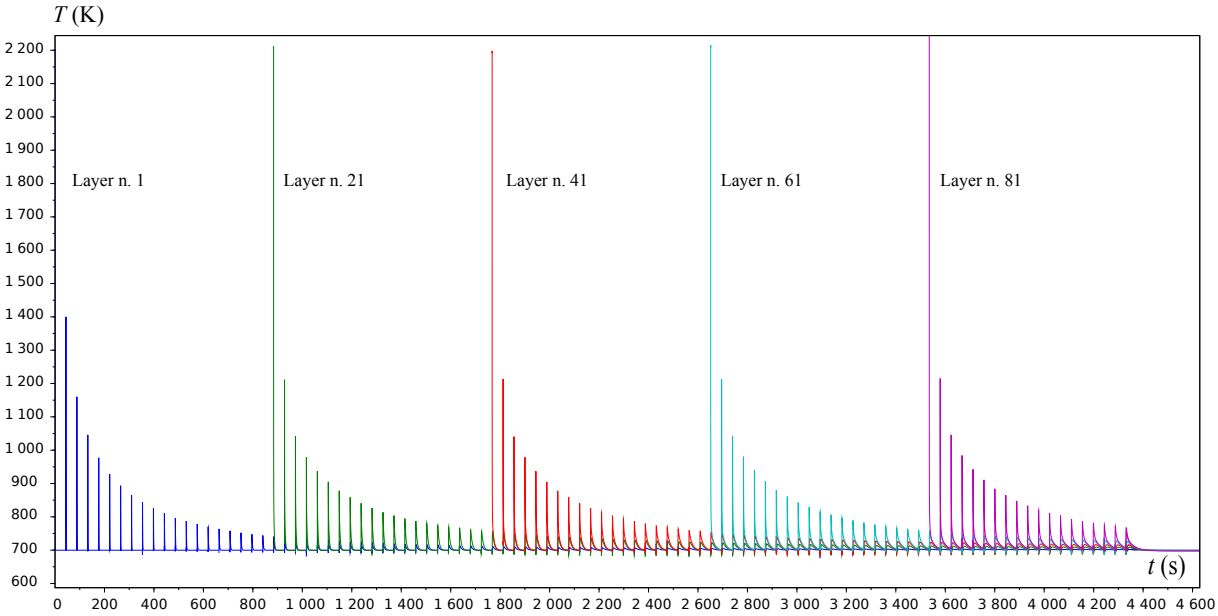

Figure 4: Temperature evolution of some layers, computation 2

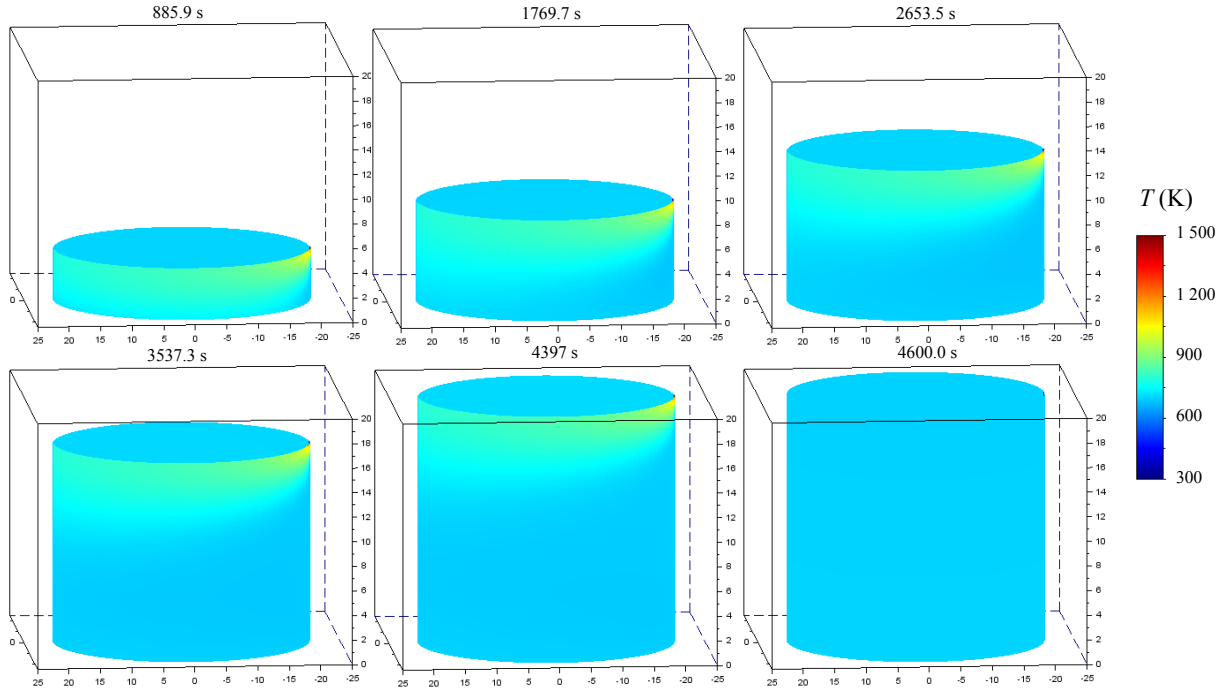

Figure 5: Temperature field, computation 2

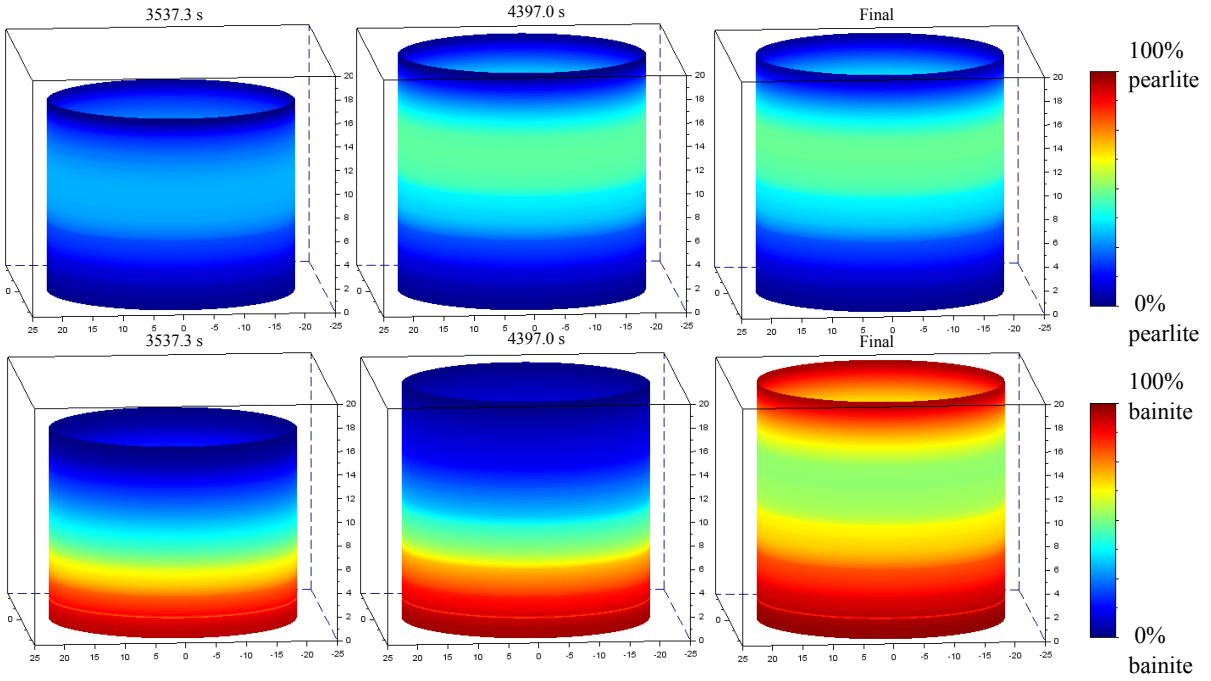

Figure 6: Phase proportion field, computation 2

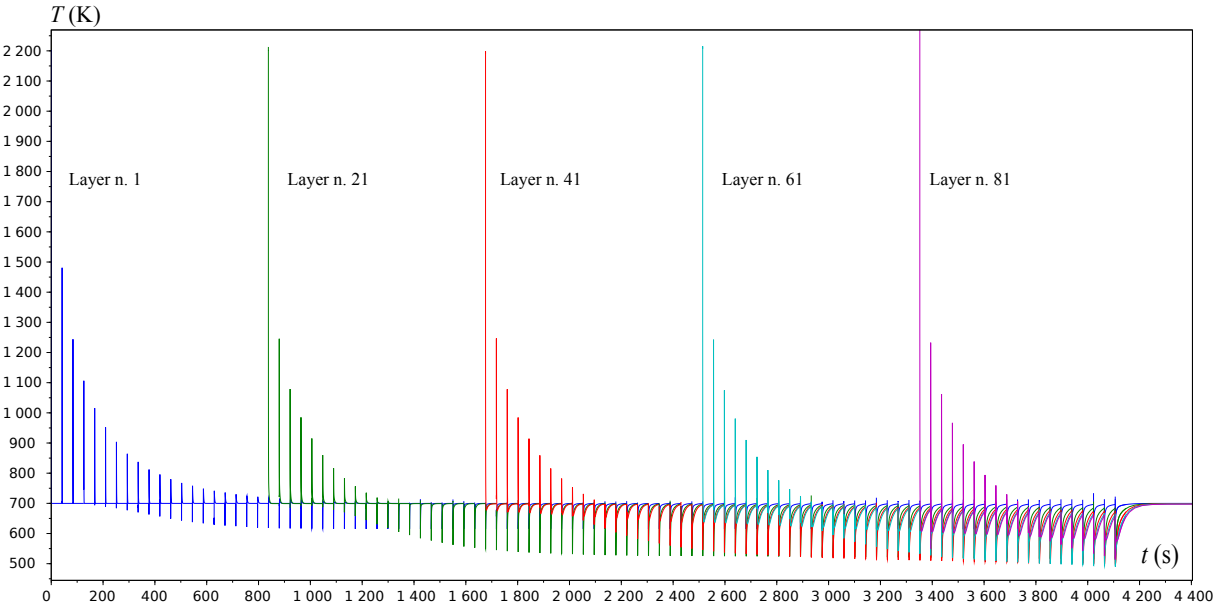

Figure 7: Temperature evolution of some layers, computation 3

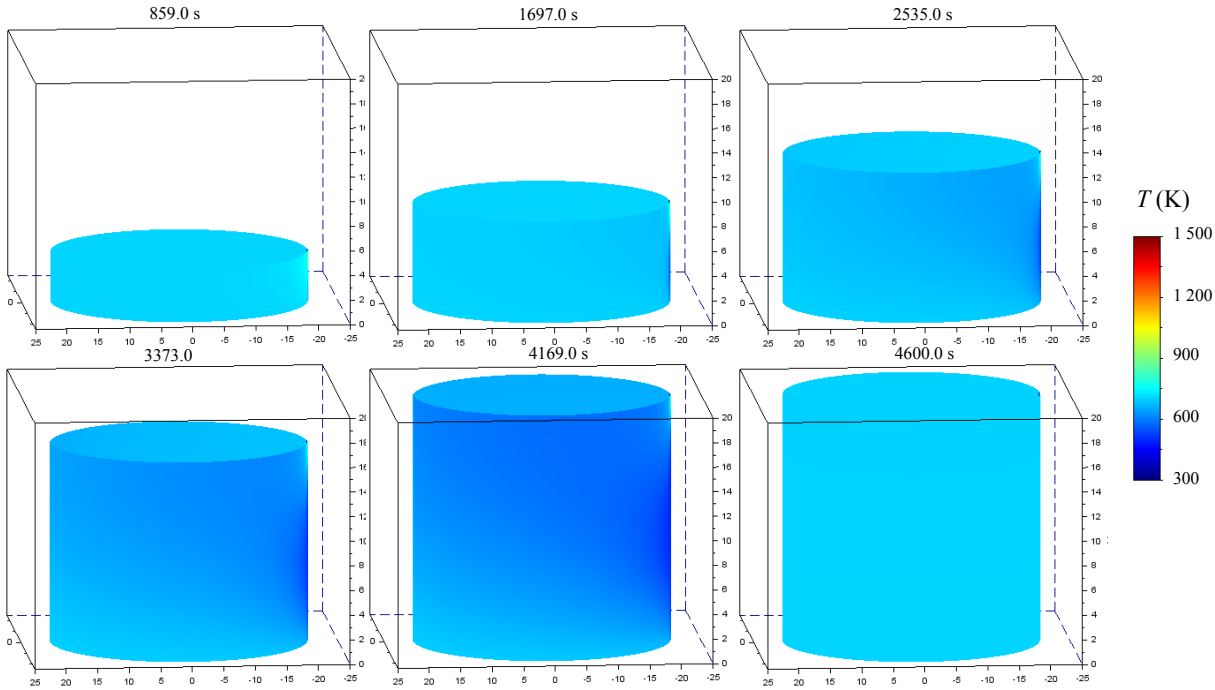

Figure 8: Temperature field, computation 3

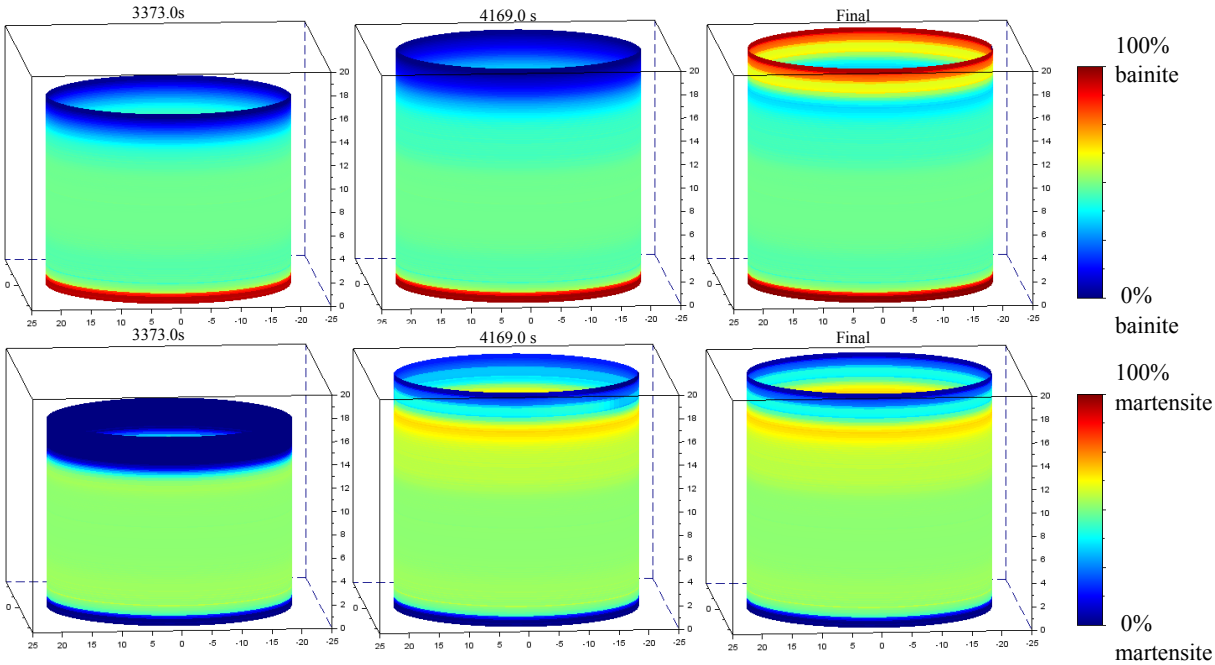

Figure 9: Phase proportion field, computation 3